Computational Fluid Dynamic Analysis to investigate methanol synthesis on the commercial catalysts

M. Bazai[a], H. Bazai[b], A. Mirvakili[c1], M.R. Rahimpour[a2]

[a] *Department of Chemical Engineering, School of Chemical and Petroleum Engineering, Shiraz University, Shiraz 71345, Iran*

[b] *Department of Mechanical Engineering University of Pretoria Hatfield, 0028 Pretoria, South Africa*

[c] *Chemical Engineering Department, Faculty of Petroleum, Gas and Petrochemical Engineering, Persian Gulf University, Bushehr, Iran 75169-13817*

Abstract:

In this study, a novel plate methanol reactor (shell and plate) with a higher heat transfer rate relative to its conventional counterparts (shell and tube) was investigated. In fact, in the new configuration, all the tubes were replaced with plates, and thereby the heat transfer area increased. To compare the two configurations (the conventional reactor (CR) and the plate reactor (PLR)), a two-dimensional computational fluid dynamics (CFD) model was developed. To draw a more meaningful comparison, an equal amount of catalyst was considered for both configurations. The modeling results were also compared with available industrial data, illustrating a good agreement. Results also showed that the main superiority of the PLR was its higher methanol production, which was about 1.2% greater than that of the CR. Besides, the obtained temperature of reactant gas and coolant gas in PLR, respectively, was 13 °C more and 9 °C less than CR. This result implies that the increase in the surface area in PLR can increase the heat transfer rate, and thereby increasing the methanol production.

Keywords: Tubular Reactors; Plate Reactors; Methanol Production; CFD; Heat Transfer

[1] Coressponding author: mirvakili@pgu.ac.ir; mirvakili96@gmail.com
[2] Corresponding author: rahimpor@shirazu.ac.ir
(H.Bazai Email: Bazaee.Hassan@Gmail.com)

1. Introduction

Methanol

Methanol is one of the most important chemical products all over the world[1-3]. This combustible liquid is the simplest alcohol with numerous applications and derivatives such as dimethyl ether, formaldehyde, methyl formatted, and acetic acid. Methanol can mainly be produced from natural gas, wood, and coal. Besides, it is known as a strategic product due to its usage as the jet engine fuel [4-6].

Generally, methanol production processes are divided into two main categories involving high-pressure and low-pressure methods [7-10]. It should be noted that low-pressure processes are more preferable than high-pressure ones because of their advantages such as less required power to compress the gas and also a longer lifetime of catalysts. Moreover, designing exchangers with more capacities and lower required operating pressure is feasible under low-pressure processes.

These processes themselves have three different sections including synthesis gas production, methanol production, and methanol distillation.

Nowadays, the methanol production industry has gained considerable attention due to its numerous applications and therefore lots of researchers have dealt with this subject. By way of illustration, Graff et al. [11]simulated a low-pressure methanol production reactor using the commercial Cu-Zn-Al catalyst. Their results showed that the intra-particle diffusion limitations depend on the size of the catalysts particles. There are some CFD modeling studies in the methanol production process and the application of methanol which had been carried out by researchers[9, 12]. For example, Lovik [13]investigated the modeling, estimation, and optimization of a methanol production reactor in the presence of a deactivated catalyst to develop a moderately accurate equilibrium

model. In addition, Flavio Manenti et al. [14]proposed a dynamic model for a fixed-bed methanol reactor, and compared the results to the equilibrium state. Rahimpour et al. [15] performed a numerical optimization for a dual-type reactor which was membrane-assisted. They showed that using the optimal operating conditions, maximization of methanol production with the proposed structure is possible. Rahimpour et al. [16] in another study introduced a new fluidized-bed reactor with a hydrogen perm-selective membrane to produce Methanol, and they could enhance methanol production efficiency by 9.53 % using the proposed structure the proposed structure resulted in a 9.53% enhancement in the efficiency of methanol production. Rahimpour et al. [17] also modeled a two-stage Lurgi methanol production reactor in both co-current and counter-current flow patterns, and according to the modeling results, the co-current flow reactor had a lower conversion and longer catalyst lifetime compared to the counter-current flow reactor. In another study, Peter et al. [18] investigated various kinetic models for the synthesis of methanol on a copper ternary catalyst. Accordingly, the power low model and pseudo-mechanistically Langmuir-Hinshelwood-Hougen-Waston model are more accurate in the estimation of issues such as the diffusion limits during Methanol synthesis, while the micro-kinetic model includes morphological changes that are very important in the synthesis of Methanol. Bhatliya et al. [19] conducted a three-dimension simulation for methanol production reactor with a shell and tube configuration using CFD software.

However, because of the complexity of the heterogeneous, exothermal reactions related to methanol production, evaluating the effects of the shell structure, the temperature of the coolant gas, as well as the heat transfer behavior is of paramount importance. For this purpose, Hosseini et al. [20] simulated an industrial multi-tube methanol reactor by CFD method. In their study, the phase distribution, temperature distribution, pressure drop, and water circulation rate were

estimated. The obtained results then were compared with the corresponding industrial data, confirming the reliability of the proposed model. Furthermore, Mirvakili et al. [21] simulated a dual-type reactor for the methanol production to evaluate the effects of flow patterns using CFD software. From the simulation results, it was found that mal-distribution of the temperature after four years of operation could be attributed to the non-uniform flow distribution in the shell and tube. Likewise, Rahmatvand et al. [22] developed a model for a fixed-bed Lurgi catalytic reactor in which an adiabatic reactor was employed instead of a gas-cooled one. Moreover, a condenser was implemented between the adiabatic and the water-cooled reactors to hinder the condensation of the gas as an operational problem associated with the gas-cooled reactor. In addition, the high diameter to length ratio of adiabatic reactors caused a slight pressure drop along the reactor and improved the conversion of carbon dioxide to methanol, which can also exert positive environmental effects. Rahmatmand et al. [19] substituted a plate reactor for the tubular water-cooled one, and applied four adiabatic beds before the water cooled reactor. Their simulation results showed that methanol production increased, carbon dioxide emission reduced and catalyst life time enhanced.

Process description

Conventional Reactor (CR)

To increase the methanol production efficiency, Lurgi Company designed a dual-type methanol reactor which consists of a gas-cooled reactor (GC) along with a water-cooled reactor (WC). The gas-cooled one is an isothermal reactor in which a part of the synthesis gas is converted to the methanol. The temperature of the produced methanol is higher than of earlier synthesis reactors

(one-stage reactors). Initially, the fresh synthesis gas enters the tubes of GC from the bottom. In the meanwhile, the outlet of WC enters GC's shell from the top, where the catalysts are present and methanol production exothermic reaction occurs. The generated heat from the exothermic reaction is transferred to the gas flowing inside the tube of GC to increase its temperature. After that, the heated gas inside the GC's tubes is entered to the WC's tubes, which are filled up with the catalyst particles, where the methanol synthesis reaction takes place, providing simultaneous reactions in both WC and GC. The main difference between the two mentioned reactions is that here in WC, the generated heat is transmitted to the shell of the reactor where is full of saturated water, and consequently causes the production of saturated vapor. The unreacted synthesis gas exiting the WC enters the GC's shell to further push the methanol synthesis reaction towards completion. . Eventually, the generated methanol is sent to the distillation unit to be purified.

Plate Reactor (PLR)

According to Fig. 1, the unit schematic of methanol production has been shown based on Lurgi's synthesis methanol arrangement which involves two types of reactors: the first one is gas-cooled and the second one is water-cooled.

The used amount of catalyst in both PLR and earlier gas-cooled (CR) reactors is equal.

To draw a better comparison, the appropriate amount of catalyst for PLR is estimated by calculating the height which is equivalent to CR in addition, the inlet conditions are exactly the same. The geometric characteristics of both reactors are presented in Table 1.

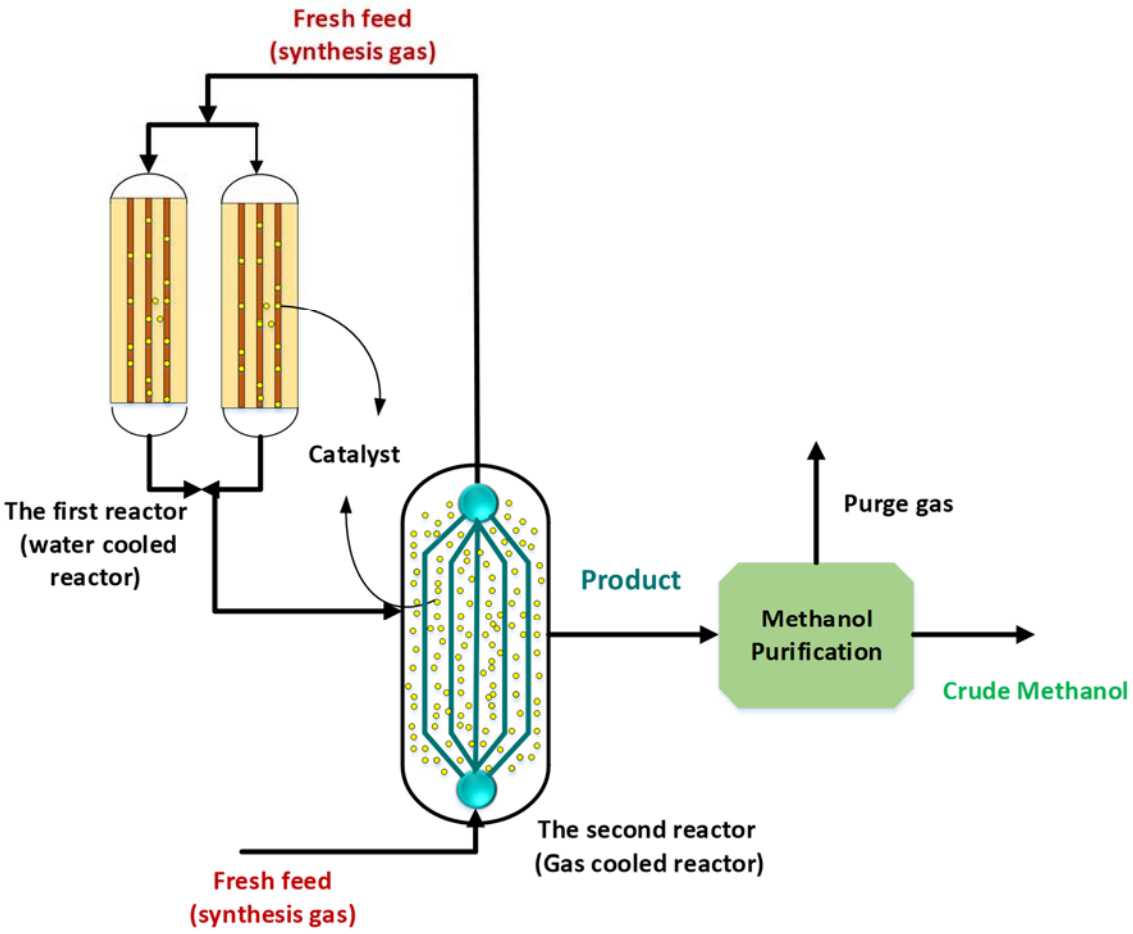

Figure 1: Schematic diagram of methanol synthesis unit

Table 1: Geometric properties of conventional and modern gas-cooled reactors

	Conventional reactor	**Modern reactor**	
parameter	amount	amount	unit
Tube diameter	0.0254	_	M
Shell diameter	0.0994	_	M
Tube length	10	_	M
Inner plate thickness	_	0.0026	M
Outer plate thickness	_	0.0398	M
Plate depth	_	0.76	M
Plate length	_	2.56	M

Table 2: Catalyst properties of conventional and modern gas-cooled reactors

Parameters	Values
Manufacturer	J.M(UK)
Trade Name	51-9S
Chemical Components	CuO:64% - Al_2O_3:10% - ZnO:24% - MgO:2%
Density	1.46 Kg/Liter
Shape	Cylindrical Pellets
Dimensions	Diameter (mm) = 5.4 , Height (mm) = 3.6
Average Cush Strength	> 170 KgF (Axial) – 170 KgF (Horizontal)

Objective

The conventional configuration of methanol reactors (CR) is usually shell and tube. As mentioned before, in this study, a novel methanol reactor is investigated in which plates are substituted for tubes, and thus it is called a plate reactor (PLR). The main differences between these two configurations are in their heat transfer term which arises from their different structures. To make these differences clear, a two-dimensional simulation for the fluid flow of PLR around a tube and its catalytic surrounding is performed via CFD software. Moreover, a two-dimensional simulation for the fluid flow of a PLR's plate, which is identical to the modeled CR in terms of catalyst mass and inlet condition, is carried out. Finally, the temperature and composition profile of both configurations are compared. Moreover, a comparison is made between the results of the modeling and industrial data, which demonstrates a good agreement.

The main goal of this study was comparing conventional reactor with modern reactor in terms of energy and pressure drop. PLR is the newest types of reactors in producing Methanol. CFD study of this reactor has not been performed by researchers. Therefore, as a novelty, we compared these two reactors by CFD tools.

2. Computational model

Model geometry and mesh independency

The gas-cooled reactor of conventional configuration has 0.5 m diameter and 5.470 m length. It consists of 3026 tubes with a 2.54 cm diameter and a 10 m length.

To compare the performance of shell and tube reactor with that of the PLR, a part of both configurations is chosen as the following:

From the CR configuration, a tube of gas-cooled reactor is chosen with the length of 10 m, inner diameter of 0.0254 m, and outer diameter of 0.0994 m. From the modern reactor, a plate with inner thickness of 0.0026 m, outer thickness of 0.0398 m, depth of 0.76 m, and length of 2.56 m, and its surrounding are chosen (see Figs.2 and 3).

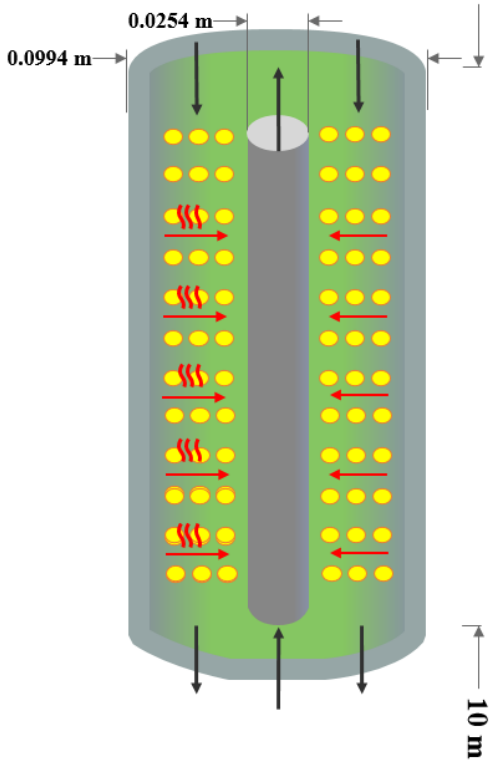

Figure 2: a three-dimensional schematic diagram of the simulated conventional reactor

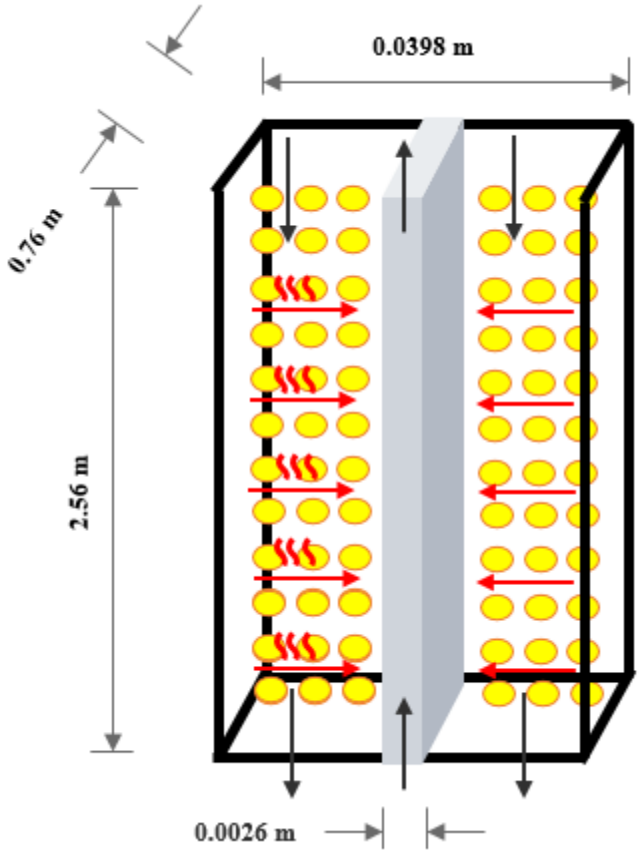

Figure 3: a three-dimensional schematic diagram of the simulated modern reactor

Because of the assumption of uniform catalyst distribution in both configurations, the thermal diffusion can be neglected in the axial direction. Moreover, regarding the dependence of turbulent flow on the motion direction, and the fact that there is no motion along the length, the thermal bulk can be neglected in this direction as well. Therefore, both systems can be modeled two-dimensionally because of the high computational costs of a three-dimensional analysis. The schematic diagrams of both systems are depicted in Figs. 4 and 5.

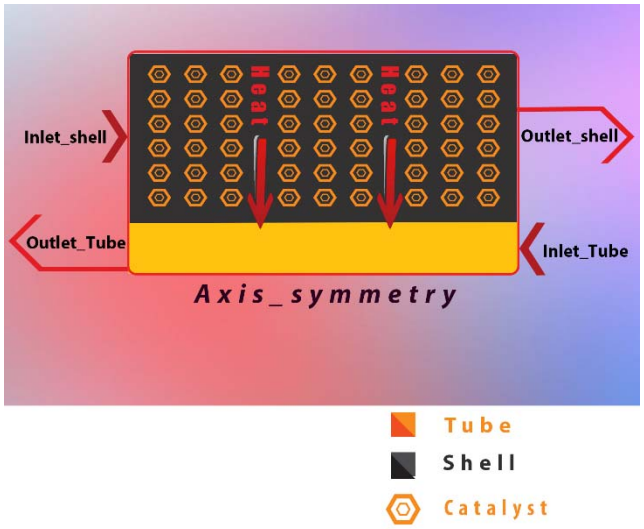

Figure 4: a two-dimensional schematic diagram of the simulated conventional reactor

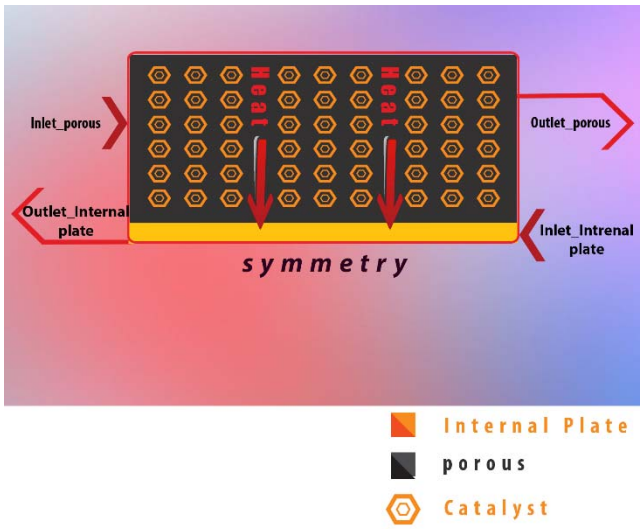

Figure 5: a two-dimensional schematic diagram of the simulated modern reactor

To perform mesh independence, we generated 4 different numbers of meshes for each reactor. For CR, 21000, 42000, 84000, and 128000, and for PLR, 190,000, 379,000, 650000, and 900000 were chosen. After comparing the results to each other, in CR and PLR, the numbers 42000 and 379000 have been selected, respectively. It is because the higher number of these amounts had the same outcome as the selected meshes.

The mesh development is done by ICEM CFD software using 42,000 meshes for CR and 379,000 meshes for PLR. The mentioned numbers are enough for the independency of the computational results on the mesh numbers.

The mesh quality of CR and PLR, respectively, is 0.98 and 0.99, illustrating the high quality of meshes.

To guarantee the independence of the results from the element size and mesh topology, mesh independency analysis is conducted by the comparison of the area-weighted average temperature of the reactant flow in the CR for four grids with the specific element size of 0.25, 0.5, 1.0, and 2.0 (cm). The results indicate that the element size of 1.0 (cm) is reliable, whereas the smaller size of cells bring about similar results, with the expense of longer computational time (due to significant number of elements). The outcomes of mesh independency from the size of cells are presented in Fig. 6. Also, the optimal size of the grid independency is used for the PLR.

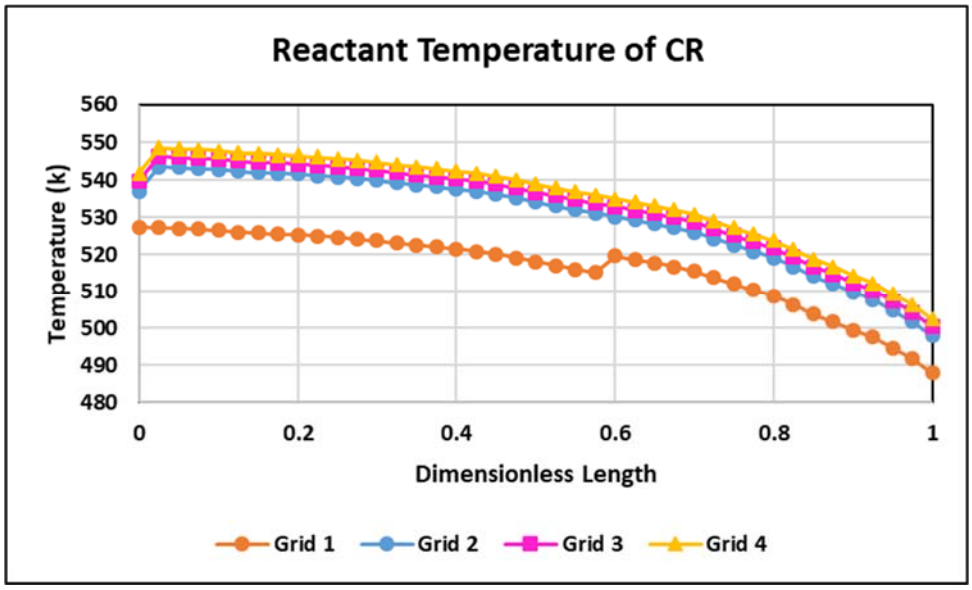

Figure 6: The results of grid independency for Grid 1(2 cm), Grid 2(1 cm), Grid 3(0.5 cm), and Grid 4(0.25cm) for CR

Numerical models

For the numerical simulation of the fluid flow in the reactor, a computational code is written. In this respect, mass, momentum, energy, and component conservation equations[23] are used as given in the following (Equations (1) to (14). Another point to mention is that a standard two-equation realizable k-Ɛ model [24] (see Equations (15) to (18)) is used for the turbulent flow.

Continuity equation

$$\frac{\partial(\rho u_i)}{\partial x_i} = 0 \tag{1}$$

Momentum equation

$$\frac{\partial(\rho u_i)}{\partial x_i} = -\frac{\partial p}{\partial x_i} + \frac{\partial \tau_{ij}}{\partial x_j} \tag{2}$$

In the equation above, fluid density, static pressure, stress tensor are shown by ρ, p, and τ_{ij}, respectively, which can be counted by equation below:

$$\tau_{ij} = \mu(\frac{\partial u_i}{\partial x_i} + \frac{\partial u_{ij}}{\partial x_i}) - \frac{2}{3}\mu.\delta_{ij}.divV \tag{3}$$

The molecular viscosity in equation above is shown by μ. Moreover, the second term on the right side of the equation is used to consider the effect of volume dilation.

Energy equation

Generally, there is spatial and temporal temperature gradients in catalytic reactors, which arise from chemical reactions heat effects in addition to transferred heat via the reactor wall. Consequently, the appropriate energy conservation equation is usually considered as:

$$\frac{\partial}{\partial x_i}\left[u_i(\rho E+p)\right]=\frac{\partial}{\partial x_i}\left[k_{eff}\frac{\partial T}{\partial x_i}-\sum_j h_i J_j+u_j(\tau_{ij})_{eff}\right]+S_h \tag{4}$$

Where the effective thermal conductivity is shown by k_{eff} and the diffusion flux of component j is shown by J_j. The conductive energy transfer, component diffusion, and viscous dissipation, respectively, are shown by first three terms on the right side of the equation. The heat of chemical reaction is shown by S_h. The E term on the left side can be calculated by the equation below.

$$E=h-\frac{p}{\rho}+\frac{u_i^2}{2} \tag{5}$$

With the aim of using equation above, the equation of sensible enthalpy which is shown by h is required as the following:

$$h=\sum m_j h_j \tag{6}$$

In this equation, m_j is used to show mass fraction of component j and h_j can be calculated as the following:

$$h_j=\int_{T_{ref}=298.15}^{T} C_{p.j}\,dT \tag{7}$$

Component conversion equation

Not only the fluid flow, but also chemical reactions between the components are important in multi-component mixtures. These reactions can be characterized by additional partial differential equation sets. Consequently, each component's mass in mixture follows a conservation law which leads to the following equation:

$$\frac{\partial(\rho u_i m_i)}{\partial x_i} = -\frac{\partial J_{ij}}{\partial x_i} + R_i \tag{8}$$

Where the mass fraction of the i component in the mixture is shown by m_i and the total rate of production arising from homogeneous chemical reactions is shown by R_i. Terms of the diffusion mass flux which is caused by concentration gradients (i.e., J_{ij}) are usually simulated by the following equation:

$$J_{i.j} = -\rho D_{m,i} \frac{\partial m_i}{\partial x_i} \tag{9}$$

In which for the component i, the diffusion coefficient in the mixture is shown by $D_{m,i.}$

Methanol synthesis from the syngas is mainly carried out based on reactions presented below:

$$CO_2 + 3H_2 \Leftrightarrow CH_3OH + H_2O \qquad \Delta H_{298} = -49.43 \frac{kJ}{mol} \tag{10}$$

$$CO + H_2O \Leftrightarrow CO_2 + H_2 \qquad \Delta H_{298} = +41.12 \frac{kJ}{mol} \tag{11}$$

Graaf et al. [11, 20, 25] presented a kinetic model which contained Hydrogenation of CO and CO_2 and the WGS reaction. They designed 18 reactions with the assumption of being elementary for each, and then they chose the best one. The presented model is available in the following:

$$r_1 = \frac{k_1 K_{CO}\left[f_{CO} f_{H_2}^{3/2} - f_{CH_3OH} / f_{H_2}^{1/2} K_{P1}\right]}{\left(1 + K_{CO} f_{CO} + K_{CO_2} f_{CO_2}\right)\left[f_{H_2}^{1/2} + \left(K_{H_2O} / K_{H_2}^{1/2}\right) f_{H_2O}\right]} \tag{12}$$

$$r_2 = \frac{k_2 K_{CO_2}\left[f_{CO_2} f_{H_2}^{3/2} - f_{CH_3OH} f_{H_2O} / f_{H_2}^{3/2} K_{P2}\right]}{\left(1 + K_{CO} f_{CO} + K_{CO_2} f_{CO_2}\right)\left[f_{H_2}^{1/2} + \left(K_{H_2O} / K_{H_2}^{1/2}\right) f_{H_2O}\right]} \tag{13}$$

$$r_3 = \frac{k_3 K_{CO_2}\left[f_{CO_2} f_{H_2} - f_{H_2O} f_{CO} / K_{P3}\right]}{\left(1 + K_{CO} f_{CO} + K_{CO_2} f_{CO_2}\right)\left[f_{H_2}^{1/2} + \left(K_{H_2O} / K_{H_2}^{1/2}\right) f_{H_2O}\right]} \quad (14)$$

The constants of reaction rate, adsorption equilibrium, and reaction equilibrium which are used in mentioned kinetic formulation above are presented in Table 3.

Table 3: The constants of reaction rate, adsorption equilibrium, and reaction equilibrium used in mentioned kinetic formulation

K=Aexp(B/RT)		
	A	*B*
k_1	$(4.89 \pm 0.029) \times 10^7$	$-63{,}000 \pm 300$
k_2	$(1.09 \pm 0.07) \times 10^5$	$-87{,}500 \pm 300$
k_3	$(9.64 \pm 7.30) \times 10^6$	$-152{,}900 \pm 6800$
K_{CO}	$(2..16 \pm 0.44) \times 10^{-5}$	$46{,}800 \pm 800$
K_{CO2}	$(7.05 \pm 1.39) \times 10^{-7}$	$61{,}700 \pm 800$
$(K_{H_2O} / K_{H_2}^{1/2})$	$(6.37 \pm 2.88) \times 10^{-9}$	$84{,}000 \pm 1400$
$K_P = 10^{(\frac{A}{T-B})}$		
	A	*B*
K_{P1}	5139	12.621
K_{P2}	3066	10.592
K_{P3}	-2073	-2.029

Turbulent model

To solve a broad diversity of the fluid flow problems, a standard k-Ɛ model is generally used with the underlying basis of similarity assumption between the viscous and Reynolds stresses on the mean flow. Though the results of the model had appropriate precision for simple flows, the

mentioned model has been modified for complex flows, which is named realizable k-Ɛ model. The realizable k-Ɛ model transport equations are available below:

$$\frac{\partial}{\partial x_i}(\rho k u_j) = \frac{\partial}{\partial x_i}\left[\left(\mu + \frac{\mu_t}{\sigma_k}\right)\frac{\partial k}{\partial x_j}\right] + G_k + G_b - \rho\varepsilon - Y_M + S_k \tag{1105}$$

$$\frac{\partial}{\partial x_i}(\rho \varepsilon u_j) = \frac{\partial}{\partial x_i}\left[\left(\mu + \frac{\mu_t}{\sigma_\varepsilon}\right)\frac{\partial \varepsilon}{\partial x_j}\right] + \rho C_1 S_\varepsilon - \rho C_2 \frac{\varepsilon^2}{k + \sqrt{v\varepsilon}} \tag{1116}$$

$$\mu_t = pC_\mu \frac{k^2}{\varepsilon} \tag{1127}$$

$$C_\mu = \frac{1}{A_0 + A_s(\frac{kU}{\varepsilon})} \tag{18}$$

In this model, a new formula for the turbulent viscosity is applied, and therefore the coefficient of dynamic viscosity is not constant.

Boundary conditions

The boundary conditions of both plate and conventional reactors are presented in Table 4 and 5.

Table 4: Catalyst characteristics (for both reactors)

Parameter	Value	Unit
Diameter	0.0054	M
Length	0.0036	M
Bed Porosity	0.34	-

Table 5: Feed characteristics (for both reactors)

Feed condition	Entered gas to the tube (and inner plate)	Entered gas to the shell (and outer plate)	Unit
Carbon monoxide (%)	8.68	4.78	-
CO_2 (%)	8.49	7.96	-
Hydrogen (%)	64.61	58.15	-
Methane (%)	9.47	10.57	-
Nitrogen (%)	8.05	9.13	-
Water (%)	0.1	1.79	-
Methanol (%)	0.37	7.17	-
Argon (%)	0.23	0.45	-
Mass flow rate	0.82	0.82	kg/s
Inlet temperature	401	537	K
Outlet pressure (gauge)	74	69	Bar

Numerical method

To solve the equations, Fluent software is used. The software is based on finite-volume model (FVM). Moreover, for coupling of pressure-velocity SIMPLE procedure is used. Therefore, on each grid of pressure calculations a try and error procedure are applied. For discretizing of all equations on computational domain second order method have been applied. Also, the residuals are set at 10^{-6} for all equations, except for energy equation that is set at 10^{-9}. To define the reaction rates (i.e., eq. 12, 13, and 14) a UDF code is written.

Model Validation

A validation of the simulated model of the CR with industrial data is presented in Table 5. Also, Fig. 8 shows the contour of the average temperature for the CR. Results of validation indicates that simulation results agree very well with the industrial data.

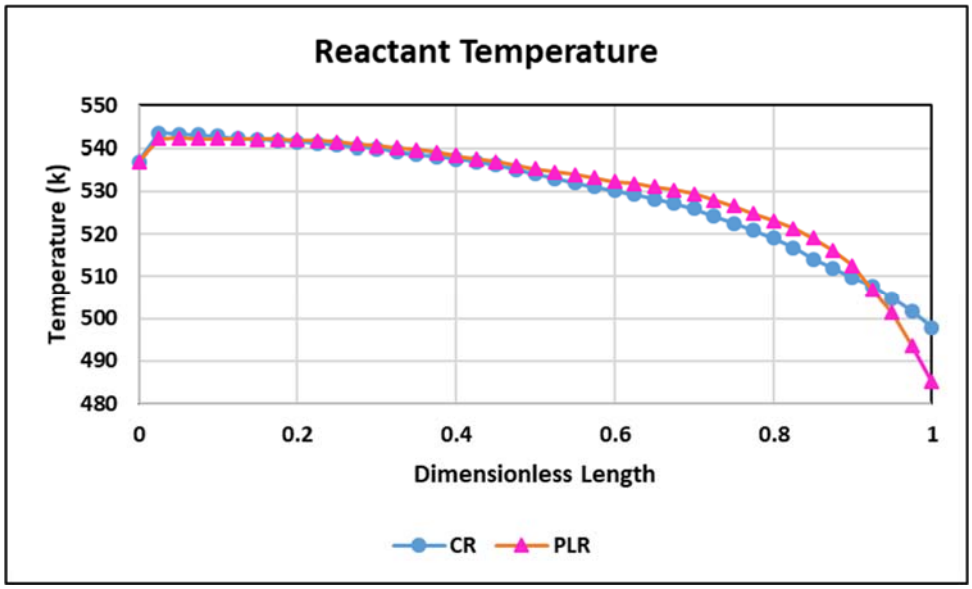

Figure 7: A comparative diagram of the gas and reactant temperature in terms of length in the conventional (CR) and modern reactors (PLR)

Table 6: The validation of the simulated model of the CR with industrial data

Temperature validation with design data			
Plant(k)		**Simulation(k)**	**Error (%)**
Thermocouple (A)	537.2	543.3	1.13
Thermocouple (B)	536.5	542.2	1.06
Thermocouple (C)	538.8	541.1	0.42
Thermocouple (D)	537.2	536.9	0.11
Thermocouple (E)	533.4	527.2	1.16
Thermocouple (F)	511.9	507.7	0.82
Cooling Gas	513	523.2	1.9
Reactant Gas	497.9	487.9	0.02
Mole Fraction With design data			
Plant		**Simulation**	**Error (%)**
Methanol	0.106	0.111	4.71
Carbon monoxide	0.025	0.021	16
Hydrogen	0.58	0.54	6
Water	0.023	0.024	4.3

3. Results and discussion

In this part of study, the temperature and concentration distributions in the gas-cooled reactor are evaluated via CFD modeling for both CR and PLR configurations.

As it is obvious in Fig. 7, there are temperature peaks for both configurations at shorts length from the reactor length, which can most likely be attributed to the extremely exothermic reactions of methanol production at the top of both reactors. Following that, the temperature of reactant gas decreases because of the heat transfer to the gas that flows inside the tube. The coolant gas is entered counter-currently with the reactant gas, so it has its lowest temperature at the inlet of the tube. On the other hand, the reaction which happens inside the shell is exothermic. Therefore, the maximum temperature gradient between the coolant and reactant gases is seen at the end of the shell where also the inlet of tube is. Consequently, the slope of the temperature-length diagram for the reactant and the coolant is higher at the outlet and inlet of the reactor.

The PLR provides more heat transfer to the gas that is inside the plate compared to the CR due to its higher heat transfer area for an equal catalyst loading. As a consequence, the outlet gas of PLR is cooled to a lower temperature than CR, and correspondingly the coolant gas of PLR is warmed to a higher temperate than CR. To illustrate, the reactant gas temperature decreases from 537 K to 484.9 K and 497.9 K for the PLR and the CR, respectively.

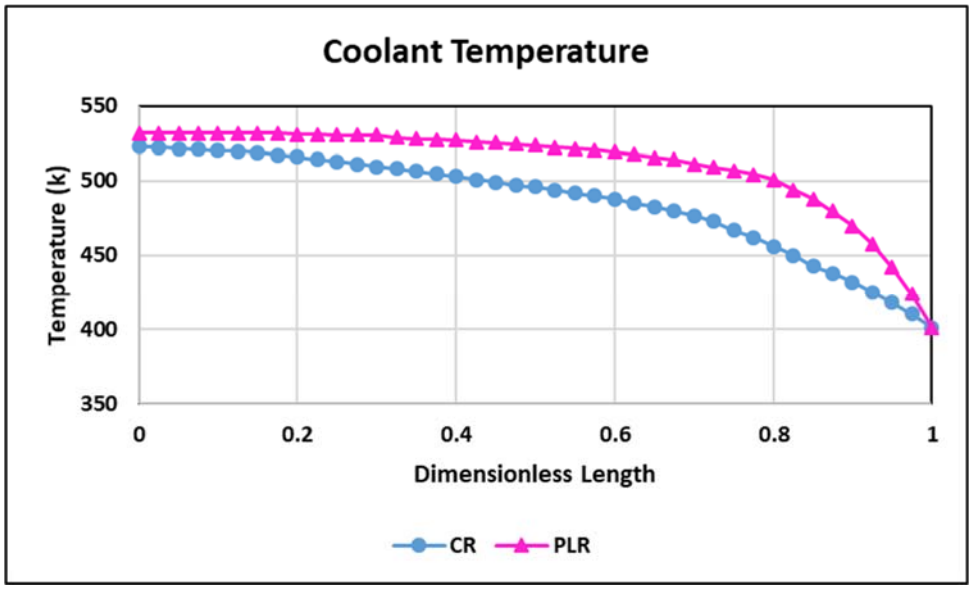

Figure 8: Comparative temperature diagram of the coolant gas in terms of length in the conventional (CR) and modern reactor (PLR)

As it can be seen in Fig. 8, the coolant gas temperatures of both reactors are increased as a result of the absorbed heat from the shell side. Moreover, the slope of the temperature diagram at the inlet of the tube is sharper than its outlet. This can be ascribed to the higher temperature gradient between the gases which are inside the tube and inside the shell at the inlet of the tube in this section. As it is clearly observed, elevated rate of heat transfer in the PLR induces more increase in the coolant gas temperature compared to the CR.

The coolant gas temperature is raised from 401 K to 523.2 K and 532.2 K for the CR and PLR, respectively.

Figs. 9 & 10 clearly reflect the ascending and descending temperature gradients for the coolant gas and reactant gas, respectively, in both reactors.

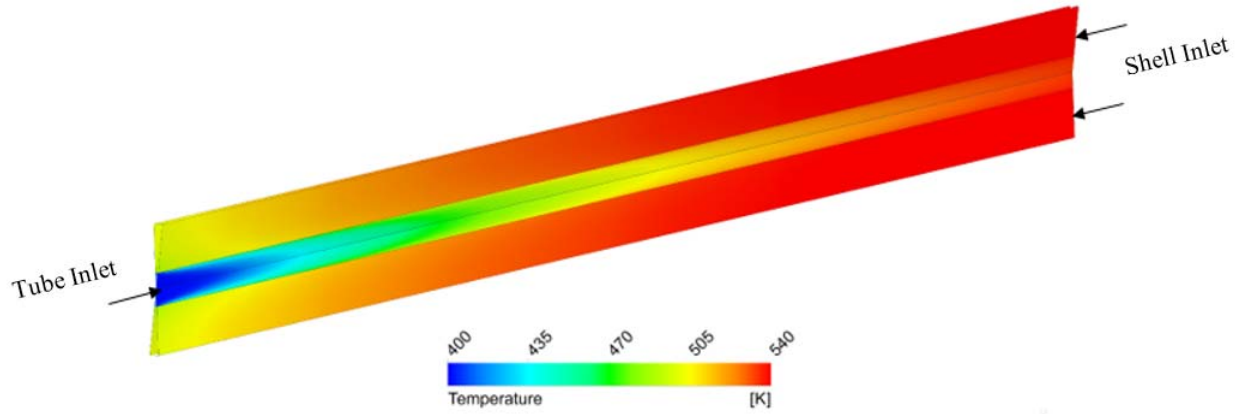

Figure 9: Average temperature contour of the conventional reactor (CR)

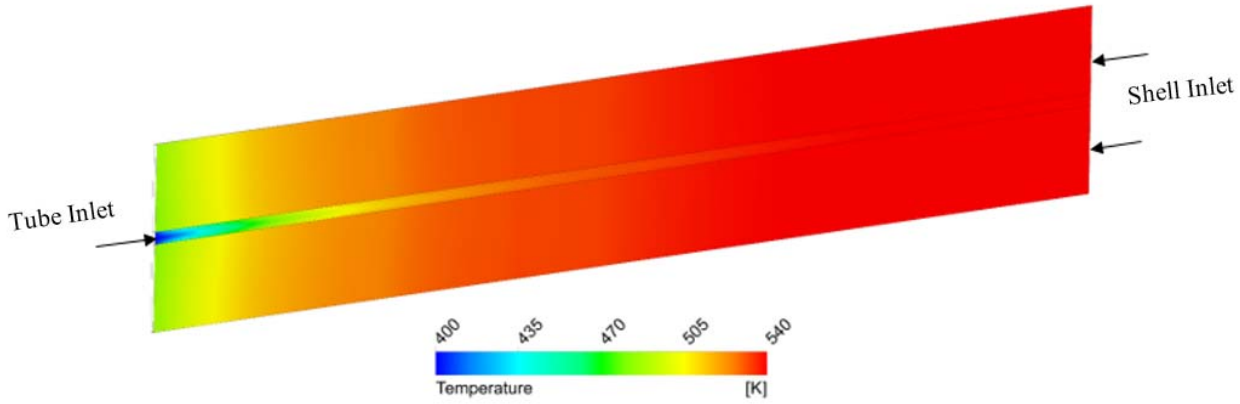

Figure 10: Average temperature contour of the modern reactor (PLR)

Fig. 11 illustrates that the molar fractions of the methanol increases along the length of both reactors, increasing from 0.072 to 0.111 and 0.123, for CR and PLR, respectively. Additionally, due to the greater rate of heat transfer in the PLR compared to the CR, the methanol molar fraction is generally higher in PLR.

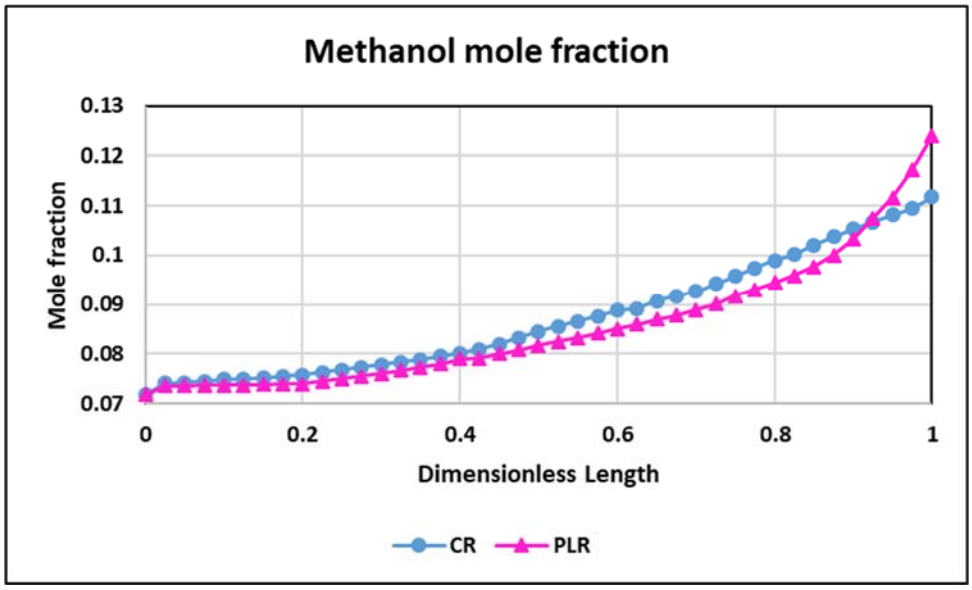

Figure 11: Comparative diagram of methanol (CH_3OH) molar fraction in the conventional (CR) and modern reactors (PLR)

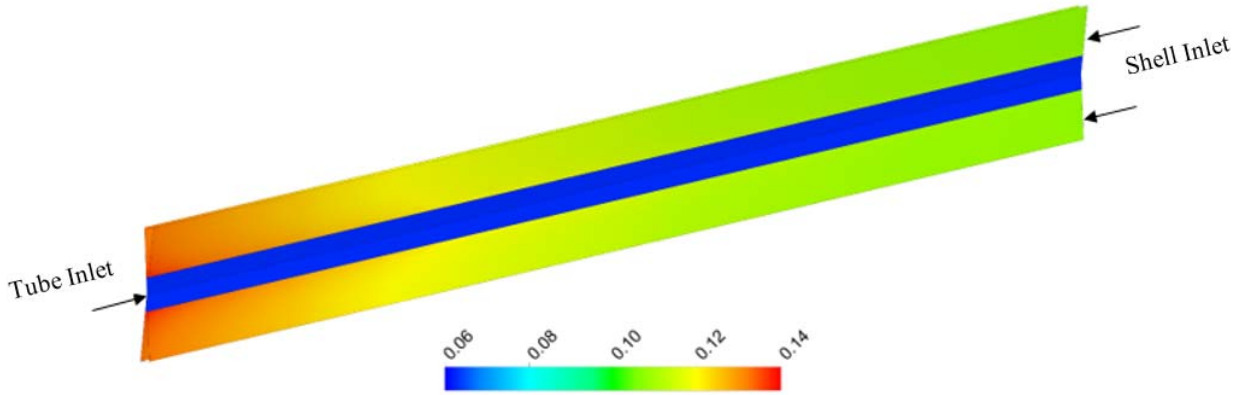

Figure 12: Contour of the methanol (CH_3OH) molar fraction in the conventional reactor (CR)

According to Figs. 13 and 14, it is obvious from the color diversities that the methanol molar fraction is boosted for the catalyst parts of both reactors which can be attributed to the methanol production reactions. Another observation is that there is no color diversity in the tube of both

reactors since no reaction occurs there. It can also be seen that the methanol molar fraction in PLR is higher compared to the CR.

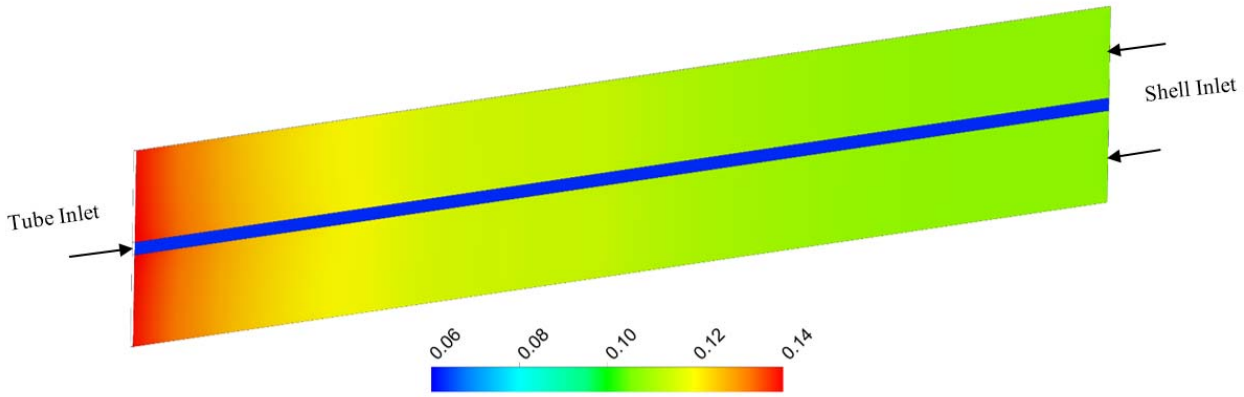

Figure 13: Contour of the methanol molar fraction in the modern reactor (PLR)

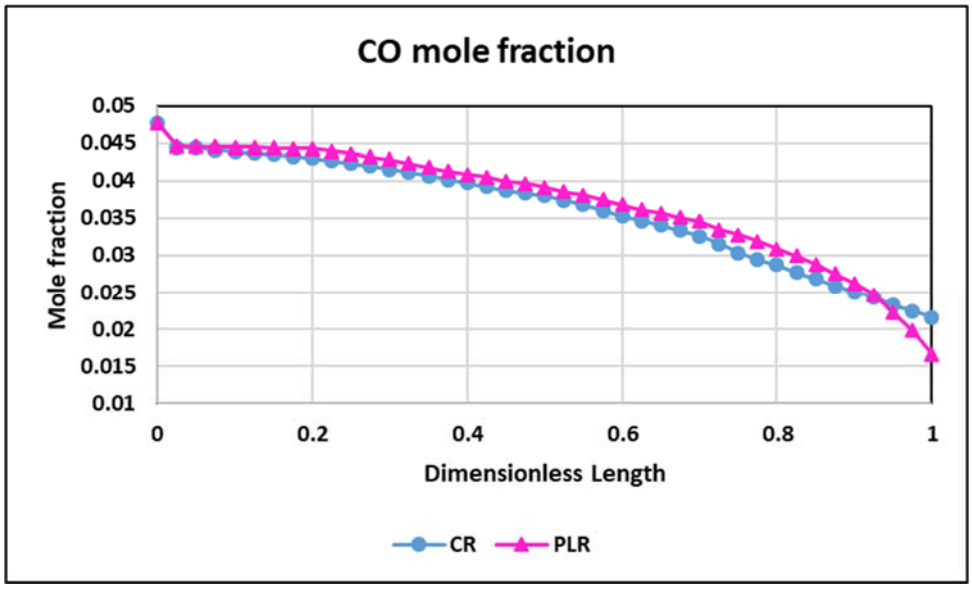

Figure 14: Comparative diagram of carbon monoxide molar fraction in the conventional (CR) and modern reactors (PLR)

Considering that carbon monoxide is a reactant component of methanol synthesis reactions, its molar fraction declines along the reactor length as it can obviously be seen in Fig. 15. In addition,

as explained before, since the methanol production rate in PLR is larger than in CR, the CO consumption rate is higher correspondingly, and thus its molar fraction is lower in PLR.

The molar fraction of carbon monoxide decreases from 0.0476 to 0.016 in PLR, while that of CR declines to 0.021.

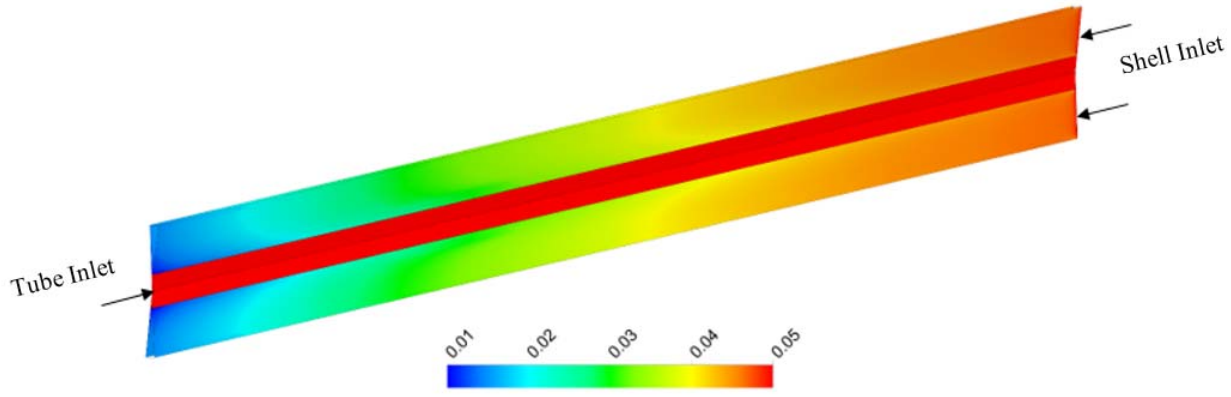

Figure 15: Carbon monoxide (CO) molar fraction contour in the conventional reactor (CR)

According to Figs. 16 and 17, carbon monoxide molar fractions decrease for both reactors in reaction section (Shell) which confirm its consumption during the reaction. In contrast, regarding the inner sections where no reaction occurs, no color change is detected. Generally, the molar fraction of carbon monoxide in PLR is lower than CR which can be explainable by more methanol production of PLR.

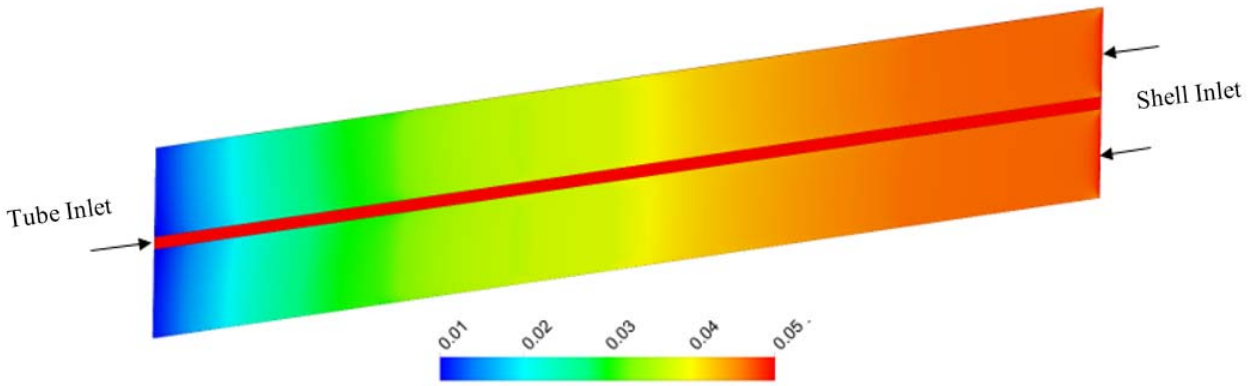

Figure 16: Carbon monoxide (CO) molar fraction contour in the modern reactor (PLR)

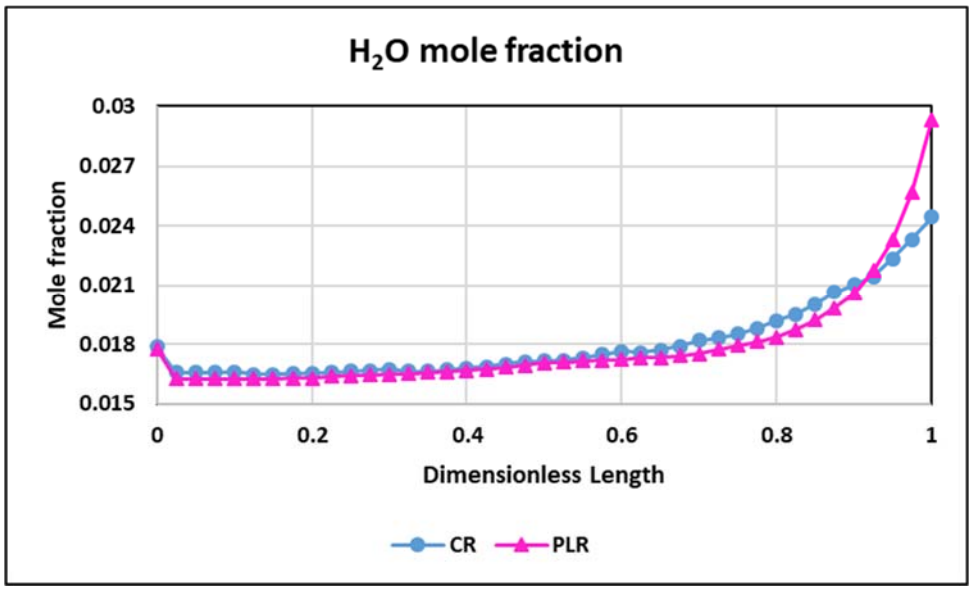

Figure 17: Comparative diagram of water molar fraction in the conventional (CR) and modern reactors (PLR)

Water molar fractions of both configurations are presented in Fig.18. It can easily be seen that in both configurations, at short distances from the top, the molar fraction of water decreases due to the water gas shift reaction, but for longer distances, it tends to increase. As expected, the molar fraction of water in the PLR is generally higher than in CR, arising from higher rate of heat transfer in the PLR.

The water molar fraction in CR and PLR increases c from 0.017 to 0.024 and 0.029, respectively.

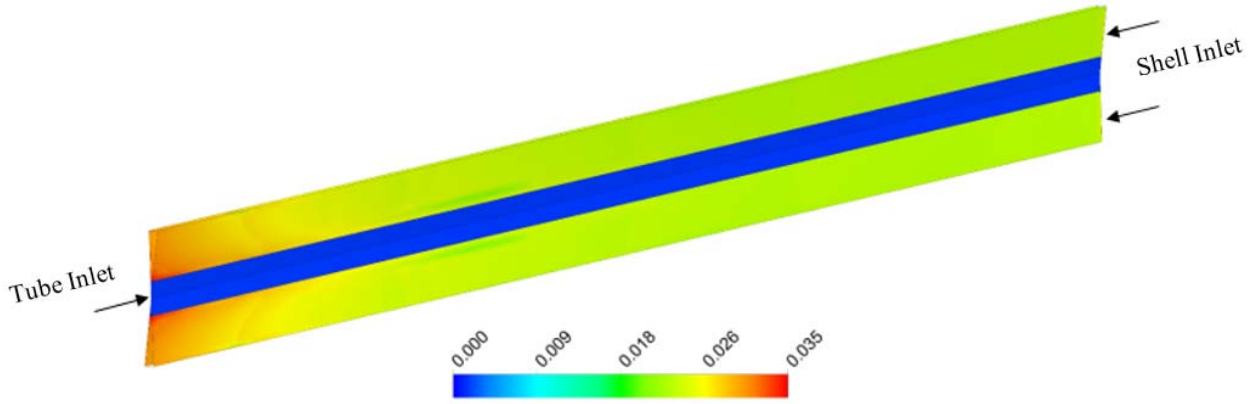

Figure 18: Contour of water (H_2O) molar fraction in the conventional reactor (CR)

Figs. 19 and 20 approve that water is generated in methanol production reaction, and typically the water generation in PLR is more than in CR.

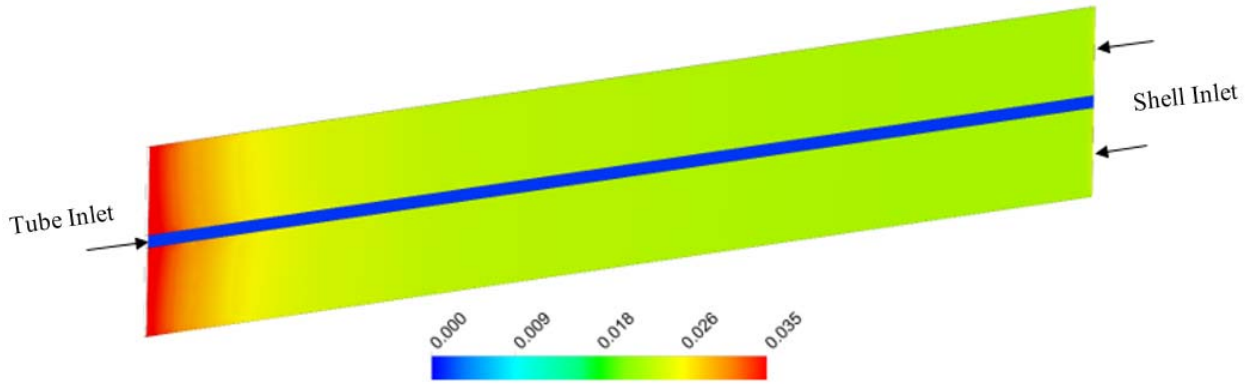

Figure 19: Contour of water (H_2O) molar fraction in the modern reactor (PLR)

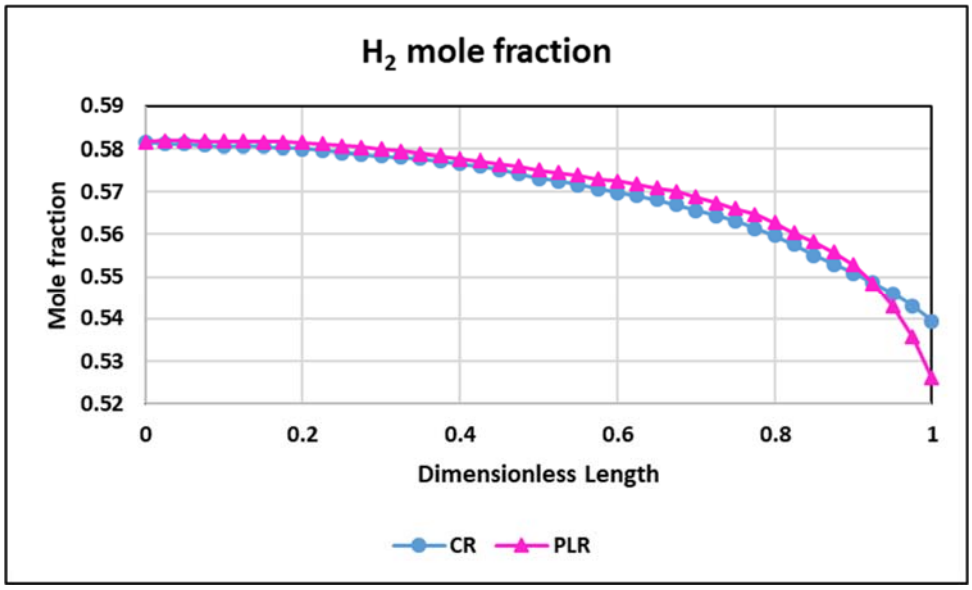

Figure 20: Comparative diagram of hydrogen (H_2) molar fraction in conventional (CR) and modern reactors (PLR)

The molar fractions of hydrogen for both configurations are presented in Fig. 21. In both cases, the concentration of hydrogen decreases along the process. Since higher rate of methanol is produced in PLR, greater rate of hydrogen consumption can be seen. The hydrogen molar fraction of CR and PLR increases from 0.58 to 0.53 and 0.52, respectively.

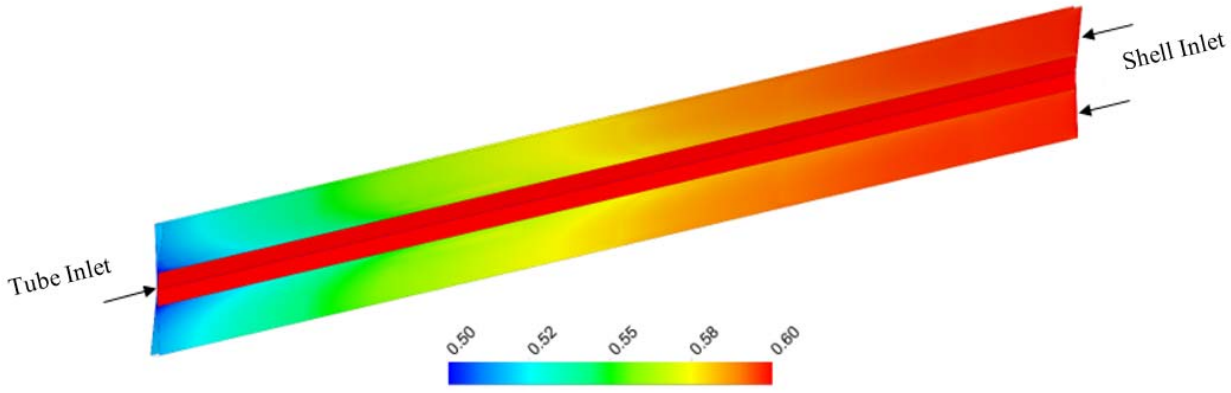

Figure 21: Contour of hydrogen (H_2) molar fraction in the conventional reactor (CR)

As it is obvious in Fig. 22 , the molar fraction of hydrogen decreases in the reaction section of both reactors, confirming the hydrogen consumption along the reactor length. It is worth mentioning that there is no color diversity due to the fact that no reaction takes place there. Totally, the hydrogen molar fraction in the PLR is lower than in the CR which is because of the higher rate of methanol production in the PLR.

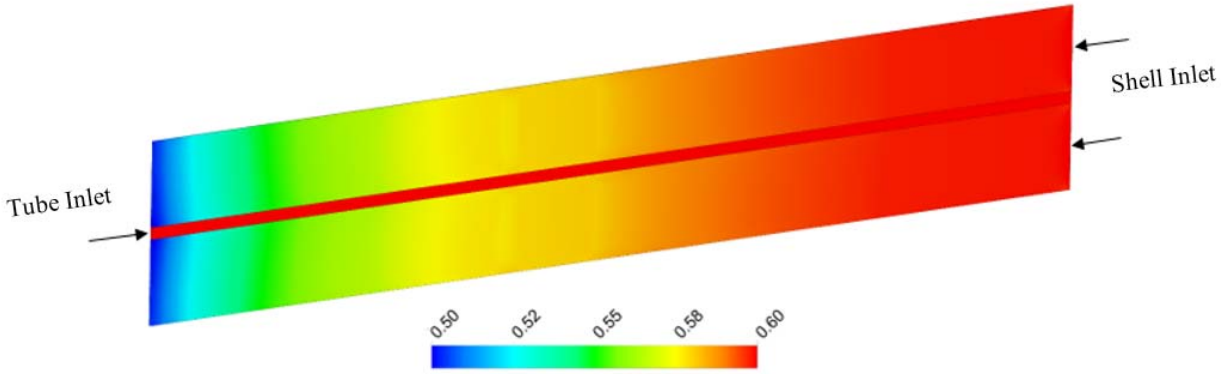

Figure 22: Contour of hydrogen (H_2) molar fraction in the modern reactor (PLR)

4. Conclusion

Results generally reveal that the PLR can give an improved performance compared to the CR, mostly because of providing a larger heat transfer area with the same catalyst loading as the CR. The superiority of PLR over CR leads to not only longer lifetime of catalysts, but also enhancement in the methanol production.

Simulation results also demonstrate that the reactant and coolant temperatures in the PLR are around 13 degrees lower, and 9 degrees higher, respectively, relative to the CR. The last point to mention is that the methanol production in the PLR is nearly 1.2% greater than in the CR.

this study shows, when the length of the reactor and the volume of catalysts are equal for both types of reactors, the production of methanol of PLR is 1.2% higher than CR. This amount will create a big difference in industrial scale. It means, in industrial scale 1.2% equals to 5000 tons/hr. Therefore, if the production rate of these two reactors is same, the length of PLR is about 50% less than CR.

References

1. El-Zeftawy, A.M., *Focus on the Chemical Value of Methanol.* Journal of King Saud University - Engineering Sciences, 1995. **7**: p. 209-254.
2. Villicaña-García, E., M.M. El-Halwagi, and J.M. Ponce-Ortega, *Involving economic incentives in optimizing the methanol supply chain considering conventional and unconventional resources.* Applied Thermal Engineering, 2020. **166**: p. 114622.
3. Murray, R. and R. Wyse-Mason, *Investigation of methanol-biodiesel-coconut oil ternary blends as an alternative fuel for CI engines.* Engineering Science and Technology, an International Journal, 2018. **21**(5): p. 1056-1066.
4. Yasari, E., *Improved dynamic performance of a thermally efficient reactor through water removal and defining new objective functions.* Fuel Processing Technology, 2019. **193**: p. 82-93.
5. Russell, R.B.B. and N.H. Rickles, *Jet turbine engine fuel, including methanol and isopropanol*. 1953, Google Patents.
6. Patel, S.K.S., et al., *Methanol production by polymer-encapsulated methanotrophs from simulated biogas in the presence of methane vector.* Bioresource Technology, 2020. **304**: p. 123022.
7. Lange, J.-P., *Methanol synthesis: a short review of technology improvements.* Catalysis Today, 2001. **64**(1-2): p. 3-8.
8. Farsi, M. and M.F. Lari, *Methanol Production Based on Methane Tri-reforming: Process Modeling and Optimization.* Process Safety and Environmental Protection, 2020.
9. Mirvakili, A. and M.R. Rahimpour, *Mal-distribution of temperature in an industrial dual-bed reactor for conversion of CO2 to methanol.* Applied Thermal Engineering, 2015. **91**: p. 1059-1070.

10. Lee, D., P. Hacarlioglu, and S.T. Oyama, *The effect of pressure in membrane reactors: trade-off in permeability and equilibrium conversion in the catalytic reforming of CH 4 with CO 2 at high pressure.* Topics in catalysis, 2004. **29**(1): p. 45-57.
11. Graaf, G., E. Stamhuis, and A. Beenackers, *Kinetics of low-pressure methanol synthesis.* Chemical Engineering Science, 1988. **43**(12): p. 3185-3195.
12. !!! INVALID CITATION !!! [7, 9, 10].
13. Løvik, I., *Modelling, estimation and optimization of the methanol synthesis with catalyst deactivation.* 2001.
14. Manenti, F., S. Cieri, and M. Restelli, *Considerations on the steady-state modeling of methanol synthesis fixed-bed reactor.* Chemical Engineering Science, 2011. **66**(2): p. 152-162.
15. Rahimpour, M. and H.E. Behjati, *Dynamic optimization of membrane dual-type methanol reactor in the presence of catalyst deactivation using genetic algorithm.* Fuel Processing Technology, 2009. **90**(2): p. 279-291.
16. Rahimpour, M., M. Bayat, and F. Rahmani, *Enhancement of methanol production in a novel cascading fluidized-bed hydrogen permselective membrane methanol reactor.* Chemical Engineering Journal, 2010. **157**(2-3): p. 520-529.
17. Rahimpour, M. and M. Lotfinejad, *A comparison of co-current and counter-current modes of operation for a dual-type industrial methanol reactor.* Chemical Engineering and Processing: Process Intensification, 2008. **47**(9-10): p. 1819-1830.
18. Peter, M., et al., *Detailed kinetic modeling of methanol synthesis over a ternary copper catalyst.* Chemical engineering journal, 2012. **203**: p. 480-491.
19. Bhatelia, T., et al. *CFD modelling of a tubular reactor for methanol synthesis*. in *Asia Pacific Confederation of Chemical Engineering Congress 2015: APCChE 2015, incorporating CHEMECA 2015*. 2015. Engineers Australia.
20. Mahmoodi, B., et al., *CFD simulation of reactor furnace of sulfur recovery units by considering kinetics of acid gas (H2S and CO2) destruction.* Applied Thermal Engineering, 2017. **123**: p. 699-710.
21. Mirvakili, A., A. Bakhtyari, and M.R. Rahimpour, *A CFD modeling to investigate the impact of flow mal-distribution on the performance of industrial methanol synthesis reactor.* Applied Thermal Engineering, 2018. **128**: p. 64-78.
22. Rahmatmand, B., M. Rahimpour, and P. Keshavarz, *Development of Two Novel Processes for Hydrogenation of CO2 to Methanol over*

Cu/ZnO/Al2O3 Catalyst to Improve the Performance of Conventional Dual Type Methanol Synthesis Reactor. Catalysts, 2018. **8**(7): p. 255.
23. Bird, R.B., *Transport phenomena.* Appl. Mech. Rev., 2002. **55**(1): p. R1-R4.
24. Shih, T.-H., et al., *A new k-epsilon eddy viscosity model for high Reynolds number turbulent flows: Model development and validation.* NASA Sti/recon Technical Report N, 1994. **95**: p. 11442.
25. Graaf, G., et al., *Intra-particle diffusion limitations in low-pressure methanol synthesis.* Chemical Engineering Science, 1990. **45**(4): p. 773-783.